Using street view images to identify road noise barriers with ensemble classification model and geospatial analysis

Kai Zhang [a,b,c], Zhen Qian [a,b,c], Yue Yang [a,b,c], Min Chen [a,b,c,d,*], Teng Zhong [a,b,c], Rui Zhu [e], Guonian Lv [a,b,c], Jinyue Yan [f,g]

[a] *Key Laboratory of Virtual Geographic Environment (Ministry of Education of PRC), Nanjing Normal University, Nanjing 210023, PR China*
[b] *State Key Laboratory Cultivation Base of Geographical Environment Evolution, Nanjing 210023, PR China*
[c] *Jiangsu Center for Collaborative Innovation in Geographical Information Resource Development and Application, Nanjing 210023, PR China*
[d] *Jiangsu Provincial Key Laboratory for NSLSCS, School of Mathematical Science, Nanjing Normal University, Nanjing 210023, PR China*
[e] *Department of Land Surveying and Geo-Informatics, The Hong Kong Polytechnic University, Kowloon, Hong Kong, PR China*
[f] *School of Business, Society & Engineering, Mälardalen University, Västerås 72123, Sweden*
[g] *Department of Chemical Engineering, KTH Royal Institute of Technology, Stockholm 10044, Sweden*

ARTICLE INFO

ABSTRACT

Road noise barriers (RNBs) are important urban infrastructures to relieve the harm of traffic noise pollution for citizens. Therefore, obtaining the spatial distribution characteristics of RNBs, such as precise positions and mileage, can be of great help for obtaining more accurate urban noise maps and assessing the quality of the urban living environment for sustainable urban development. However, an effective and efficient method for identifying RNBs and acquiring their attributes in large areas is scarce. This study constructs an ensemble classification model (ECM) to automatically identify RNBs at the city level based on Baidu Street View (BSV). Firstly, the bootstrap sampling method is proposed to build a street view image-based train set, where the effect of imbalanced categories of samples was reduced by adding confusing negative samples. Secondly, two state-of-the-art deep learning models, ResNet and DenseNet, are ensembled to construct an ECM based on the bagging framework. Finally, a post-processing method has been proposed based on geospatial analysis to eliminate street view images (SVIs) that are misclassified as RNBs. This study takes Suzhou, China as the study area to validate the proposed method. The model achieved an accuracy and F1-score of 0.98 and 0.90, respectively. The total mileage of the RNBs in Suzhou was 178,919 m. The results demonstrated the performance of the proposed RNBs identification framework. The significance of obtaining RNBs attributes for accelerating sustainable urban development has been demonstrated through the case of photovoltaic noise barriers (PVNBs).

1. Introduction

Road noise barriers (RNBs) are generally stetted between roads and buildings that are usually residential, educational, and medical areas. Construction of RNBs is an effective way to reduce traffic noise, which will adversely affect the health of residents living around highways and main roads (Dumbrava & Miah, 2016). RNBs can also be an indirect index for assessing the sustainable development degree by influencing the residential environmental quality and city landscape forms. Additionally, RNBs are promising locations that can be installed in distribution photovoltaic systems. Photovoltaic noise barriers (PVNBs) as a new form of solar energy utilized in urban areas can provide clear energy and optimization of the energy constitution. Therefore, RNBs as

sustainable transport infrastructure, make it scientific planning and construction can effectively promote the green and sustainable development of the cities (Song, Thatcher, Li, McHugh, & Wu, 2021).

With the continuous process of urbanization, the construction of urban road networks and the demand for traffic continue to increase, leading to more urgent requirements for setting RNBs (Liu et al., 2020). At the same time, grasping and mapping the spatial distribution of existing RNBs is a prerequisite for RNBs planning and construction at the city scale. In addition, the attribute information of RNBs, such as their positions and mileages, is important fundamental data for related research, such as simulating and evaluating road traffic noise pollution (Wang & Wang, 2021; Zhao et al., 2017), assessing the impact of RNBs on vehicle exhaust fluidity (Wang & Wang, 2019), and calculating the

---

solar radiation potential of PVNBs (Zimmerman, Panda, & Bulović, 2020).

However, the precise positions and mileages of RNBs in large areas are difficult to collect. Because the data are usually managed by various local governments, making it time consuming to obtain authorized data. In addition, such data created by different entities have different data structures and formats, making them even difficult to use effectively. Although the precise position and milage of an RNB can be collected by field measures (Potvin, Apparicio, & Séguin, 2019), this approach is not feasible for large geographical scales. Some researchers have deduced the RNBs mileage of the entire country based on the ratio of RNB mileage to roads in a given area (Wadhawan & Pearce, 2017). However, this result may still be very different from the actual RNB distribution characteristics in derivation areas. Therefore, it is necessary to explore feasible methods to collect the precise positions and mileages of RNBs at the city or larger scales.

Fortunately, the combination of deep learning methods and street view imaging services, e.g., Google Street View (GSV) and Baidu Street View (BSV), provide the possibility of identifying and extracting ground features efficiently and conveniently, such as urban forms, street canyon compositions (Middel, Lukasczyk, Zakrzewski, Arnold, & Maciejewski, 2019) and urban commerce distributions (Ye, Wang, Kita, Xie, & Cai, 2019). In light of the extraordinary performance of deep learning methods when combined with BSV, this study employs ensemble learning (Krawczyk, Minku, Gama, Stefanowski, & Woźniak, 2017) to construct an ensemble classification model (ECM) for automatically identifying RNBs in street views at the city scale. Ensemble learning aims to integrate data fusion, data modeling and data mining into a unified framework. The core of ensemble learning is to integrate multiple base algorithms' weak prediction results to obtain higher prediction performance on classification, detection, or segmentation tasks (Dong, Yu, Cao, Shi, & Ma, 2020). Although ensemble learning has proven its excellent performance in various fields (Pham, Kim, Park, & Choi, 2021), there is no relevant research exploring the applicability of this algorithm in RNBs identification.

Thus, this study combines ensemble learning with street view images (SVIs) to explore a quick, convenient, and low-cost method for identifying RNBs at the city scale. Compared with a previous study that focused on a single model (Zhong et al., 2021a), this study integrated various state-of-the-art deep convolutional neural networks (DCNNs) based on the bagging ensemble strategy. The performance of the RNB identifying model was significantly improved by taking advantage of each model. Additionally, this study reduces the effect of imbalanced categories of SVIs by adding confusing negative samples, which enables our model to pay more attention to feature mining of hard RNB samples to enhance the performance of RNB identification. Finally, a post-processing method based on geospatial analysis in this study has been proposed to eliminate misclassified SVIs, in which the recall and precision indicators can be improved efficiently, and the identification results are more consistent with the real situation. The remainder of this study is structured as follows. Section 2 describes the background of RNB and its collection methods. Section 3 describes the study area, data collection, and details of the proposed method. Section 4 presents the result of RNB identification and the RNBs spatial distribution in Suzhou. Section 5 demonstrates the importance of acquiring RNBs' attributes through an application case. The discussion and conclusion are presented in Section 6.

2. Literature review

2.1. Characteristics of RNBs

The precise positions, azimuths, and mileages of RNBs are the most commonly used attributes in related research. Since RNBs are installed on either one or two sides of the road, the precise position of RNBs are useful to determine the roadside equipped with the RNB and map the linear distribution of RNBs along with the road networks. For example, only by obtaining the precise positions of RNBs can an accurate 3D noise map be created, and the severity of the road noise pollution of an area with or without RNBs can be visually displayed (Alam, Ahmad, Afsar, & Akhtar, 2020). Only by clarifying the installation positions of RNBs can the diffusion modes of automobile exhaust be accurately simulated and more accurate air quality evaluation results be obtained for nearby roads (Yang et al., 2020a). The spatial distribution of the existing RNBs indirectly reflects the gap between rich and poor people and environmental equality (Potvin, Apparicio, & Séguin, 2019). In the other aspect, the mileage of an RNB is the distance from the start and end points of the RNBs along with the road. Mileage is also important for estimating solar PV potential on PVNBs (Schepper, Van, Manca, & Thewys, 2012) because the solar energy received by the RNB is significantly affected by its azimuth, size, and geographic position.

In addition, the heights, shapes, and materials of RNBs are also important attributes that have great influences on the reduction of noise pollution (Reiter, Wehr, & Ziegelwanger, 2017). Many studies have focused on comparing the performance of RNBs with different heights, shapes, and materials to effectively mitigate the hazard of traffic noise pollution for urban residents (Liu, Chen, Zhao, & Chen, 2017; Redondo et al., 2021). However, these studies have often concentrated on very small areas because the prevention and control effects of RNBs with different heights, shapes, and materials need to be tested in many positions. Recording traffic noise through devices in large areas consumes considerable time and manpower. It is unnecessary to collect the heights, shapes, and materials of RNBs in every field site because these attributes are determined by the type of RNBs, which usually do not change much on a certain road inside the city. These attributes can be collected by setting sampling points for field measurements or marking the RNBs with GSV images or BSV images after obtaining their precise positions and mileages.

In summary, the mileages and precise positions of RNBs are very important and are the most widely used data in various fields. Although the heights, shapes, and materials of RNBs are also important data for related studies, they can be acquired at a lower cost when the precise positions and mileages of the RNBs have been collected. Therefore, academic research and practical application related to RNBs will be greatly enhanced if RNBs can be collected automatically through convenient, efficient, and low-cost methods with accurate position and mileage information. These efforts will ultimately have a positive impact on sustainable urban development.

2.2. Traditional methods for obtaining RNBs attributes

At present, there are four main approaches for collecting the precise positions and mileages of RNBs. The first approach is to make field measurements in areas with RNBs. The second approach is to use GSV to manually mark the RNB positions and thenalidate the marked results with a vehicle (Potvin, Apparicio, & Séguin, 2019; Ranasinghe et al., 2019). These two approaches may be feasible ways to collect RNBs positions at the microscale, but they are not feasible at the macroscale because these methods consume considerable manpower and material resources. The third approach is to evaluate RNBs mileage through assumption or hypothesis methods at a national scale, but this method inevitably induces accumulated uncertainty in the final result.

The fourth approach is to apply RNB data from a government agency. Although some agencies, such as the Federal Highway Administration (U. S. Department of Transportation Federal Highway Administration, 2019) and the Government of South Australia Department for Infrastructure and Transport (Government of South Australia Department for Infrastructure and Transport, 2013), provide RNB statistics or sample data, their data merely record mileages, materials, and attributed administrative regions or cover only a small area. Users still cannot acquire the precise positions of RNBs in large areas. In addition, most cities have not yet released RNB data. Applicants must go through a

complicated application process required by the government to obtain such data for different purposes. There are still two more problems to constrain the practicability of these RNB data. First, the construction time of set RNB times in different sections of a city may not be the same, causing the storage formats of the RNB engineering data to be different, such as paper records and shapefiles. Second, the state of the RNB dataset managed and maintained by the government is not always updated promptly, which may affect the completeness of the collected RNB information. Therefore, it is still difficult to use RNB data managed by the local government in related research for large areas.
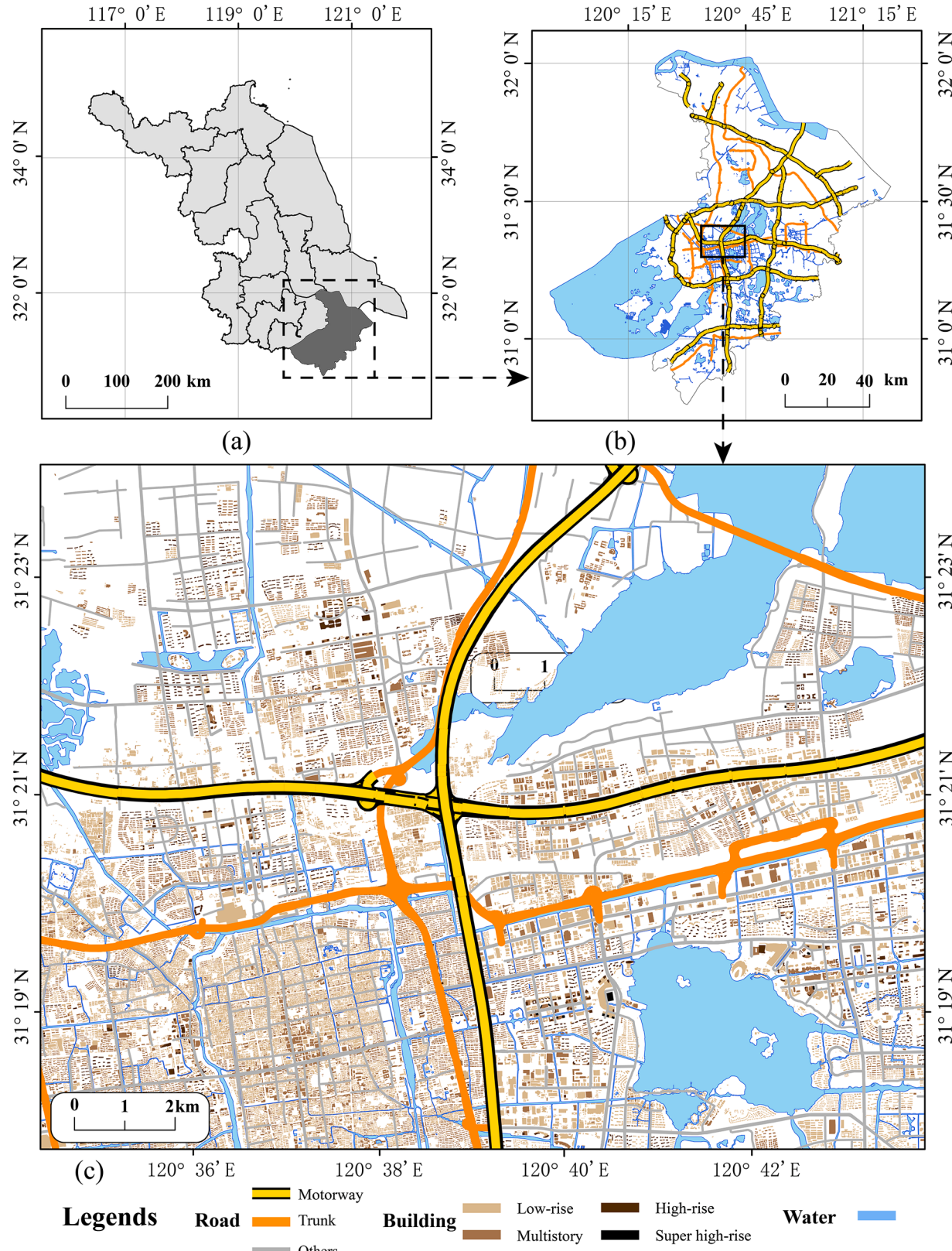

Fig. 1. Study area and experimental data. (a), (b) and (c) indicate the position of the study area, and (d) is the enlarged area corresponding to the marked box in (c), which is used to display the experimental data more clearly.
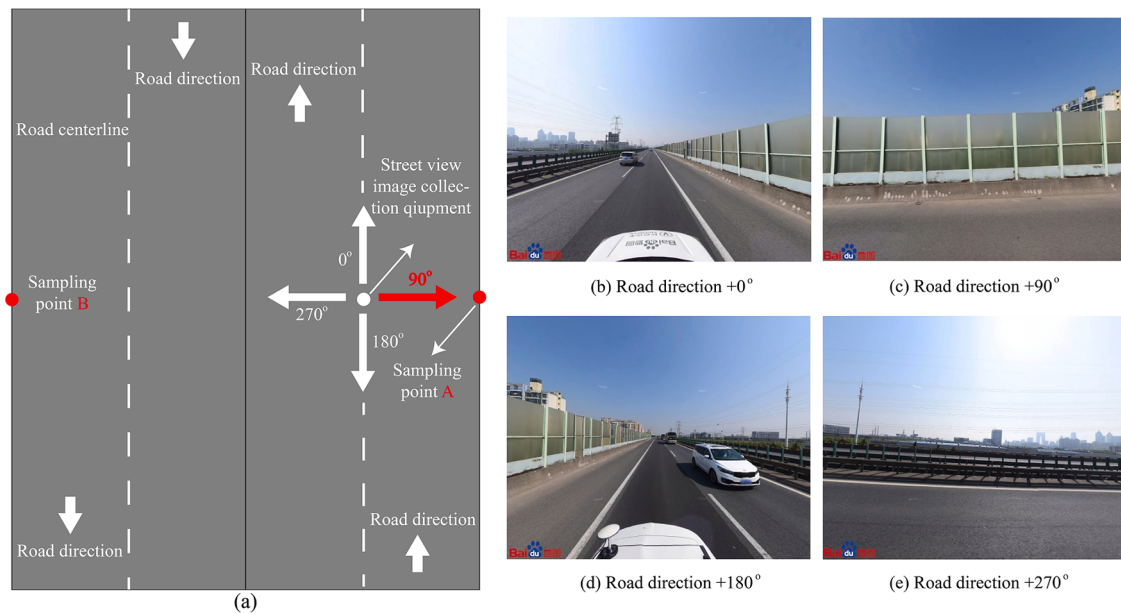
Fig. 2. Street view collection diagram. (a) indicates the sampling point position of BSV images, (b), (c), (d), and (e) illustrate the scene in four horizontal viewing angles of the BSV images.

2.3. Deep learning combined with street view imagery for ground feature detection

In recent years, deep learning has exhibited extraordinary performance in the image, speech, and natural language processing fields and has gradually been applied to city planning (Zhou, He, Cai, Wang, & Su, 2019), economic geography (Yeh et al., 2020), modern agriculture (Maimaitijiang et al., 2020) and other fields (Kang, Zhang, Gao, Lin, & Liu, 2020; Zhang, Wu, Zhu, & Liu, 2019; Zhong et al., 2021b). Image classification, object detection, and semantic segmentation models in the deep learning field combined with high-resolution remote sensing images, street view imagery, or other graphics are promising ways to address some data mining tasks (Li et al., 2021; Zhu, Shang, Hu, Yu, & Zhong, 2021). For example, the view factors of street canyons can be calculated through SVIs and semantic segmentation models (Du, Ning & Yan, 2020). Building type classification (Hoffmann, Wang, Werner, Kang, & Zhu, 2019), urban canyon geometry classification (Hu, Zhang, Gong, Ratti, & Li, 2020), crop type mapping (Yan & Ryu, 2021), urban function recognition (Ye, Zhang, Mu, Gao, & Liu, 2021), and even neighborhood demographic makeup estimation (Gebru et al., 2017) can also be implemented based on SVIs and classification, semantic segmentation, or object detection models.

However, for complex classification problems or massive data mining tasks, a single classifier that may not achieve optimal performance has been demonstrated by many studies (Chang, Abimannan, Chiao, Lin, & Huang, 2020). For example, amid air pollution forecasting, researchers contrasted the performance of hybrid models based on ensemble learning and single models (Verma, Ahuja, Meisheri & Dey, 2018). In the rockburst prediction study, the author constructed four single classical models and four ensemble models based on four single classic models pairwise ensemble, the result suggests four ensemble models had the better prediction performance than the other four single models (Yin et al., 2021). Many researchers think the reason that a single model has lower performance in data mining tasks is the imbalance of the samples, so that a single model cannot capture the object characteristics of minority classes (Díez-Pastor, Rodríguez, García-Osorio, & Kuncheva, 2015; Yuan, Xie, & Abouelenien, 2018).

It can be seen from the former literature that the lower performance of the single model in complicated classification tasks can complement rely on ensemble learning. Its main idea is to integrate the advantages of multiple individual classifiers to improve the overall performance of the machine learning in classification or data mining tasks (Wang, Wang, & Srinivasan, 2018). In the classification task, researchers used an ensemble model to propose a Weibo sentiment classification method, and they achieved higher accuracy and recall rates than the traditional model (Yang, Yuan & Wang, 2020). Other studies have also utilized decision tree-based ensemble learning and medical images to distinguish between malignant and benign tumors (Ghiasi & Zendehboudi, 2021).

Inspired by these studies, this study integrates the concept of ensemble learning into the task of RNBs recognition and builds an ECM to improve the accuracy and efficiency of RNBs recognition. Meanwhile, added the confusing negative samples when training the individual classifiers to alleviate the effect of imbalanced categories of samples to further improve the performance of the model. According to the described literature review, this research explores a convenient and time-saving method for identifying city-scale RNBs based on ECM and BSV images. The proposed method can efficiently overcome the problem regarding the lack of exhaustive and precise RNB data at the city scale, and the method can be extended to other regions based on the concept of transfer learning.

3. Material and methods

3.1 Study area

This paper takes Suzhou, Chinese as the study area to validate the reliability and performance of the proposed method for identifying RNBs. Suzhou is one of the central cities of the Yangtze River Delta (Fig. 1) and is also a national high-tech industry base in China. Suzhou has a resident population of 10.74 million and an urbanization rate of 77%, and it ranks the 6th in terms of the gross domestic product (GDP) in China in 2019 in 2019 (National Bureau of Statistics of China, 2020). With an increasing rate of urbanization in Suzhou, the city has become an important engine for the integrated and coordinated development of the Yangtze River Delta. Thus, analyzing the spatial distribution of RNBs in Suzhou is of great significance for urban noise pollution assessment and PVNBs solar energy potential assessment and application.

3.2 Experimental data collection

The road network data in Suzhou are downloaded from the open-sourced crowdsourcing OpenStreetMap (OSM). The attributes of the road network are well organized into 10 categories, such as highways, trunk roads, primary roads, and secondary roads. Based on our rigorous survey, RNBs are constructed along highways and trunk roads in urban areas. Therefore, this study only retrieves highways and trunk roads from the OSM road network.

This study creates a series of SVI sampling points on highways and trunk roads in Suzhou with 20 m constant intervals based on OSM road network data. Our pilot study has suggested that the generation of sampling points with 20 m intervals is a feasible strategy because it not only makes the scene for the continuity of the BSV images between adjacent sampling points but also decreases the storage space and the collection time required for the BSV images. According to the co-ordinates of the created sampling points, the BSV images are automatically collected from the Baidu API through a Python script. The Baidu Panorama Static Image API service provides complete documentation that allows a set of customized parameters for retrieving BSV images, including the width, height, position, heading, and collection time of each BSV image (Baidu Map Open Platform, 2021).

Highways and trunk roads are bidirectional, and RNBs are generally built along the two sides of the road. Therefore, to match noise barriers to the corresponding roadside correctly when using ECM, this study acquires BSV images with 90° viewing angles along the direction of the road. As shown in Fig. 2, if a BSV image with a viewing angle of 270° to the direction of the road is collected at sampling point B, then the BSV images at sampling point B will be misidentified as RNBs. The 270° viewing angle of sampling point B is consistent with the SVI collected at the 90° viewing angle of sampling point A. In this study, the information about each acquired BSV image is as follows: the size is 500×400 pixels, the heading (horizontal angle) is 90°, and the field of view (FOV) (horizontal range) is 90°.

When collecting the BSV images, it is found that in the viaduct areas, the BSV images on and under the bridge were collected at different time periods. However, RNBs are often installed on the bridges of viaduct areas. Therefore, collecting BSV images for only one period is likely to lead to unrecognized RNBs in the viaduct area due to the lack of BSV images collected at the viaduct. In addition, some BSV images are missing on a few road segments in a certain year. These missing images are likely to be supplemented in other years. For this reason, this study collected all the SVIs of Suzhou City from 2014 to 2020, yearly. That is, if there are SVIs of different years at the sampling point, then collect all the SVIs of these different years. As a result, a total of 148,336 sampling points are generated based on highways and trunk roads, and a total of 287,714 BSV images in Suzhou are acquired according to the designated plan of BSV image collection.

3.3 Building of ECM

The method proposed in this study consists of the following steps. First, BSV images are collected from a BSV image repository and sampling points are generated from a complete set of road networks. Then, the positive and negative samples in the collected BSV images are selected and marked. Furthermore, a group of state-of-the-art deep convolutional nerual networks are trained and integrated into an ECM through snapshot ensemble and voting. Finally, in the study area, RNBs are identified and mapped through the trained ECM. Fig. 3 shows the overall flowchart of this study.

3.3.1. Base classifiers

A classifier is a general term for sample classification methods in data mining, including algorithms such as decision trees, logistic regression, naive Bayes, and neural networks. Residual neural networks (ResNets) and dense convolutional networks (DenseNets) are state-of-the-art networks based on convolutional neural networks (CNNs). Generally, the more layers of the network, the richer the feature information extraction of the dataset. However, with the increasing number of network layers, accuracy becomes saturated and then degrades rapidly, model performance does not increase but decreases, this phenomenon is also called the degradation of networks (He, Zhang, Ren & Sun, 2015). The main contribution of a ResNet is to address the problem by which the network accuracy decreases rapidly as the number of network layers deepens by optimizing the structure of the network (He et al., 2015). Therefore, ResNet is considered one of the best CNN models for classification. ResNet101and ResNet152 have good effects on fusion, and they have excellent performance. They have the same network constructures, and the only difference is different layers of networks (Ibrahim et al., 2020).

DenseNet is a brand new network that designs dense blocks to create a narrower network, and this new network enhances the propagation of features between each hierarchy network and drastically reduces the required number of parameters, thereby making the network easier to train (Huang et al., 2016a) . DnseNet improved network performance by alleviating the degradation phenomenon and strengthening the transmission of features between layers in the networks. DenseNet161 and DenseNet201 are demonstrated to have excellent performance compared to other layers of DenseNet on detection, segmentation, and classification tasks (Alawi, Anaam, & Al-sohbani, 2021). Similar to ResNet, DenseNet161 and DenseNet201 also have the same network constructures, the only difference is that they have different layers of networks.
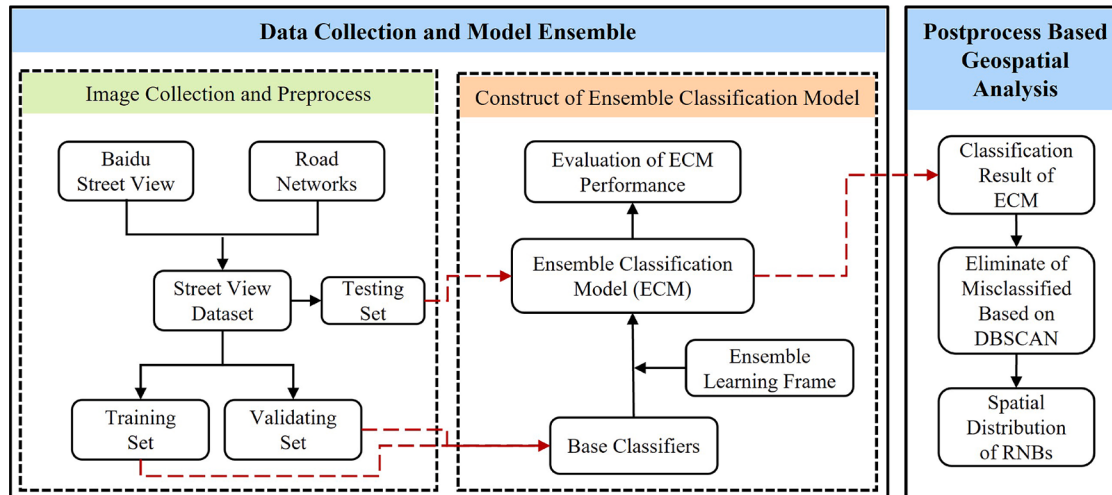

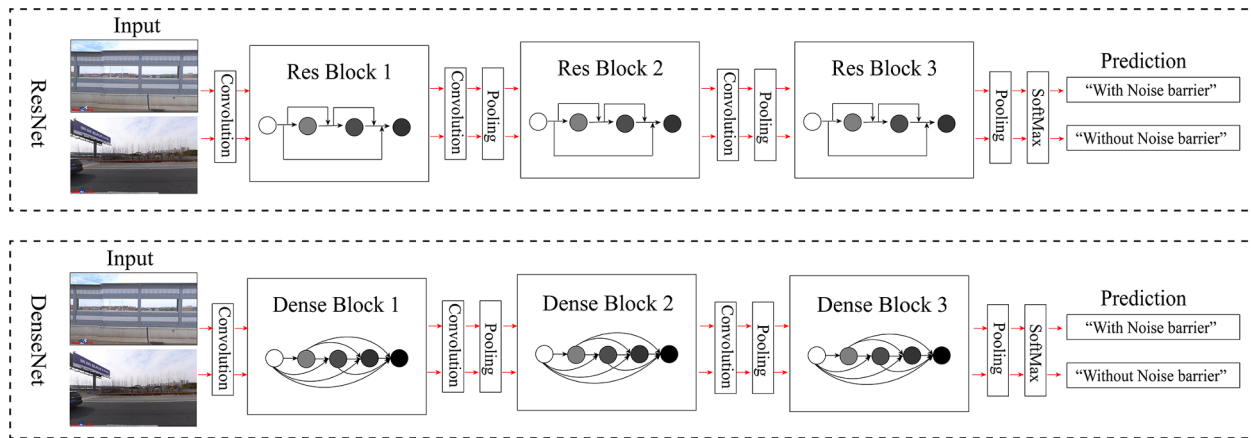**Fig. 3.** Research flowchart of PNB identification based on the ECM and SVI.

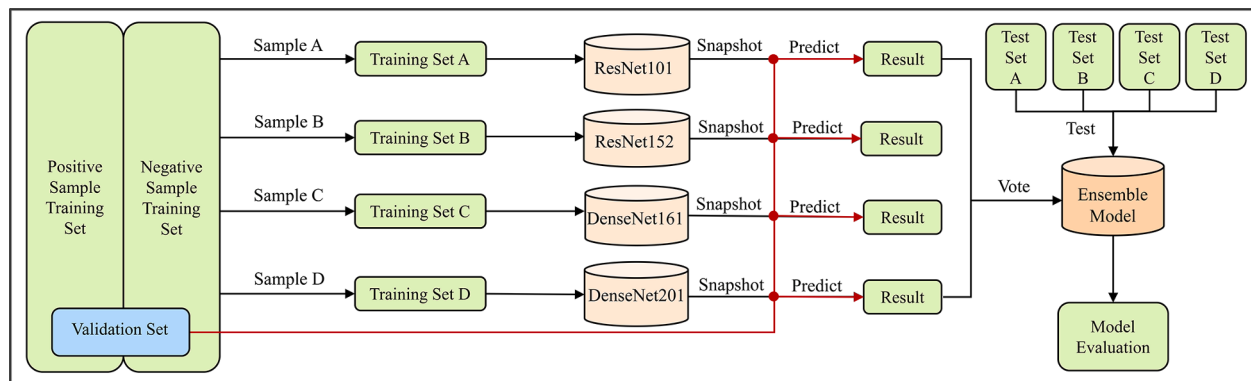**Fig. 4.** ResNet and DenseNet network structure.

Fig. 5. ECM construction and evaluation framework .

Therefore, this study integrates four state-of-the-art classifiers, ResNet101, ResNet152, DenseNet161, and DenseNet201, to identify RNBs in SVIs. The ResNet and DenseNet network structures are shown in Fig. 4. In ResNet and DenseNet network structures, the layers between two adjacent blocks are referred to as transition layers and change feature-map sizes via convolution and pooling (Huang et al., 2016a). The SoftMax layer turns the original classification score of the object into a positive normalized value for the model to judge. The main function of Res Block is to pass the residual function directly to the next layer when the feature information has been well characterized, simplifying the difficulty of model training. The main character of Dense

Block is the input of each layer comes from the output of all the previous layers. So, Dense Block connects more paths between the fore and back feature maps and retains more information to the new feature maps through residual connection.

3.3.2. Ensemble frame

Bagging is one of the mainstream ensemble frames, and it operates based on parallel strategies to construct an ensemble model. The prediction results of each base classifier are aggregated rely on the voting method. The bagging frame utilizes the boosting sampling method to construct the base classifier's training dataset (Suthar & He, 2021).
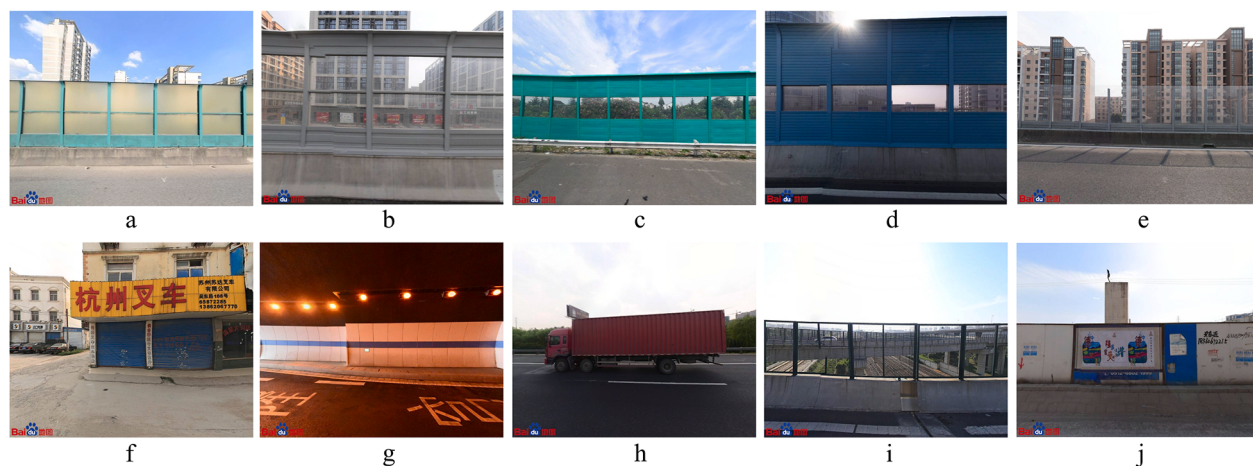

Fig. 6. Positive RNB samples (a-e) and partial classical negative samples that are easily recognized as RNBs: (f) billboard, (g) inner wall of a tunnel, (h) truck, (i) guardrail, (j) building fence.

Table 1
The form and index definition of the confusion matrix.

Realistic situation	Classification result	
	Positive examples	Negative examples
Positive examples	TP (Positive samples predicted as positive by the model)	FP (Negative samples predicted as positive by the model)
Negative examples	FN (Positive samples predicted as negative by the model)	TN (Negative samples predicted as negative by the model)

Table 2
The formula and specific definition of assessment indexes.

Formula	Meaning
$Accuraacy = \dfrac{TP + TN}{TP + TN + FP + FN}$	The ratio of the numbers of with RNBs and without RNBs BSV images that correct classified by the ECM to the total BSV images
$Precion = \dfrac{TP}{TP + FP}$	The ratio of the number of BSV images with RNBs in realistic situation to the numbers of BSV images with RNBs that classified by the ECM
$Recall = \dfrac{TP}{TP + FN}$	The ratio of the number of BSV images with RNBs in realistic situation to the numbers of correct classified BSV images by ECM
$F1 - score = \dfrac{2 \times Precision \times Recall}{Precision + Recall}$	A comprehensive evaluation of the recall and precision of ECM result

Table 3
Performance of the ensemble model and the four base classifiers .

Classifier	Accuracy	Recall	Precision	F1-score
ResNet101	0.98 ($\pm$ 0.00)	0.97 ($\pm$ 0.02)	0.79 ($\pm$ 0.02)	0.87 ($\pm$ 0.02)
ResNet152	0.98 ($\pm$ 0.00)	0.97 ($\pm$ 0.01)	0.78 ($\pm$ 0.01)	0.86 ($\pm$ 0.02)
DenseNet161	0.98 ($\pm$ 0.00)	0.97 ($\pm$ 0.02)	0.81 ($\pm$ 0.01)	0.88 ($\pm$ 0.02)
DenseNet201	0.98 ($\pm$ 0.00)	0.97 ($\pm$ 0.01)	0.81 ($\pm$ 0.02)	0.88 ($\pm$ 0.02)
ECM	0.98 ($\pm$ 0.00)	0.97 ($\pm$ 0.02)	0.83 ($\pm$ 0.02)	0.90 ($\pm$ 0.02)

Boosting-based sampling is a method that utilizes sampling with replacement or repeated sampling to create a sample dataset. The aim of boosting-based sampling is to create a training dataset that has the same size as the original sample dataset through repeated sampling, approximately 36.8% of the original samples are not extracted to the training dataset (Silva, Ribeiro, Moreno, Mariani, & Coelho, 2021). Then, the remaining samples are regarded as validation datasets to optimize the individual classifiers. These base classifiers are trained based on the existing training dataset.

Snapshot ensembles can generate a set of accurate and diverse models from one training session. When training a neural network model, it is generally necessary to set different learning rates to conduct a sensitivity analysis. However, this process requires hundreds or even thousands of epochs to complete, which means that model training will take a significantly long time. Snapshot ensembles can rely on the cosine annealing algorithm to force the model to fall into the local optimum quickly by setting different learning rates and then conserving the optimal models obtained under this learning rate (Huang et al., 2017). After that, the learning rate enters the next annealing cycle, the model escapes the current local optimal point, and the model continues to find a new optimal point. Because the models with different local optimal are stored with greater diversity, a more robust model will be established after the snapshot procedure.

The voting method integrates the prediction results of the four base classifiers for the same BSV image and votes according to the principle of the minority obeying the majority to finally determine the class of the BSV image. The classification principle of the ECM is presented in the following equation:

$$\widehat{y}_{ensemble} = sign\left(\sum_{m=1}^{n} \widehat{y_m} - \frac{n}{2} \right)$$

$\widehat{y}_{ensemble}$ is the final classification result of the ECM. $\widehat{y_m}$ is the classification result of the $m - th$ classifier. The values of $\widehat{y}_{ensemble}$ and $\widehat{y_m}$ are 0 or 1, representing negative and positive samples, respectively, n is the number of the classifiers.

3.3.3. Training and building of the ECM

The ensemble model construction process is shown in Fig. 5.

1) First, four training subdatasets, A, B, C, and D, are extracted by boosting-based sampling from the 4000 original samples. These four training subdatasets contain 2000 positive samples and 2000 negative samples. The positive and negative samples in the original training set that are not selected for the training subsets are used as the model validation set. According to the pre-experimental results of this study, some objects, such as road guardrails, billboards, the inner walls of tunnels, and trucks, are easily identified as RNBs. Therefore, the BSV images with these objects are added to the negative sample dataset to improve the performance of the ECM. The positive and partial classical negative samples are shown in Fig. 6.
2) Second, the ResNet101, ResNet152, DenseNet 161, and DenseNet 201 classifiers are used to train the sample data and validate the prediction by extracting the corresponding subtraining and validation datasets.
3) Finally, these four trained classifiers are integrated into an ECM through the snapshot ensemble and voting method.

3.3.4. ECM performance evaluation

It is an indispensable step to utilize the test dataset to evaluate the performance of the trained ensemble model. This study also utilizes multiple test sets to test the performance of the ECM. As shown in Fig. 5, this study extracts four test sets, A, B, C, and D, from all BSV images in Suzhou. The number of BSV images in each test set is 2000, and then each BSV image is manually marked when it contains RNBs. Then, the ECM receives the test dataset as input and generates the output for further analysis. Generally, the confusion matrix and four deduced indexes based on this matrix were used to evaluate the performance in the classification model. For a binary classification model, the classification result of the model will generate four categories after manual validation: true positive (TP), true negative (TN), false positive (FP), and false negative (FN). Table 1 shows the form and index definition of the confusion matrix.

The accuracy, precision, recall, and F1-score of four indexes calculated by TP, TN, FP, and FN are utilized to assess the performance of the ECM. The specific definitions of these indexes are shown in Table 2. The value ranges of accuracy, precision, recall, and F1-score are [0,1] after standardization. Among them, the F1-score is a weighted average of recall and precision. The value of these indexes closer to 1, means the better performance of the model.

Since this study uses multiple test sets to evaluate the ECM performance, the values of these evaluation indicators are in an interval. The performance of the ResNet and DenseNet base classifiers is also evaluated using these four indexes and then compared by the ECM. Under a learning rate of 0.001, the performance of the ECM and the four base classifiers in recognizing RNBs is listed in Table 3.

Table 3 shows the performance comparison results of the base classifiers and the ECM. Although the accuracy and recall of the ECM have not improved compared with these four base classifiers, the precision and F1-score of the ECM have obviously improved. The precision represents the ratio of the number of BSV images with RNB that have been correctly classified by the ECM to the number of total BSV images with RNB. The F1-score is the weighted average of recall and accuracy and is an evaluation index for the comprehensive performance of the model. Therefore, the precision and F1-score of the ECM improved, which indicates that the proposed approach has achieved a better performance than the conventional models.
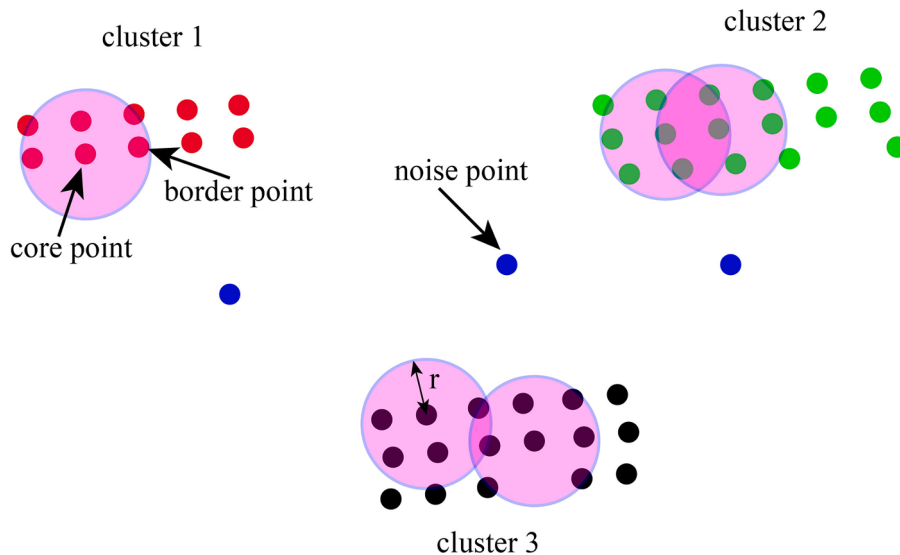
Fig. 7. Illustration of the DBSCAN cluster algorithm.

3.4. Post-process method based on geospatial analysis

All BSV images collected are input into the constructed ECM for RNB identification, and the set of BSV images with RNBs are regarded as the results of the ECM. However, the required mileage and precise position information of RNBs still cannot be acquired from the BSV images directly. To tackle this problem, this study matches BSV images with RNBs to a digital map, which is a vector map layer, and can characterize the precise positions and mileages of RNBs based on their latitude and longitude information in ArcGIS. However, even on digital maps, these BSV images with RNB are also presented in the form of points that need to be continuously processed based on collective principles of BSV images.

3.4.1. Eliminate of misclassified BSV images based on DBSCAN

Additionally, some isolated points are found when checking the BSV image points with RNBs displayed on the digital map. These isolated points are recognized as RNB, but within a few hundred meters or even thousands of meters around them, only one or two or none of them are recognized as RNB sampling points. The results show that these isolated points are misclassified as RNB when locating these points and the corresponding BSV image for artificial identification. Therefore, it is necessary to eliminate these isolated points. After these points are eliminated, the accuracy of RNB recognition will be further improved, and the distribution characteristics of RNB closer to the real urban environment will be obtained.

In this study, density-based spatial clustering of applications with noise (DBSCAN) is used to strike out the isolated RNB points. Clustering is the process of dividing samples based on the similarity between samples. DBSCAN can divide samples with a sufficient density into clusters and delete noise points that cannot be divided into a cluster. Compared with other existing clustering algorithms, DBSCAN is advanced at identifying clusters of any shape and without predetermining the number of clusters (Wang, Wang, Han, & Zhou, 2021). In addition, because the RNB points are evenly distributed along the road, the distance-based clustering algorithm is not suitable for excluding isolated points. Therefore, based on DBSCAN, these isolated points can be distinguished from the RNB points that exhibit linear clustering in a certain area to remove the misidentified RNB points, by which the performance of the ECM can be improved efficiently, and the identification results are more consistent with the characteristics of real RNBs.

DBSCAN divides original data into 3 sorts based on a threshold for the number of neighbors (Schubert, Sander, Ester, Kriegel, & Xu, 2017), *minPts*, within the radius *r* (with an arbitrary distance measure):

Table 4
RNBs identification results for Suzhou city.

BSV images in Suzhou	With RNBs	without RNBs	Isolated BSV images
287,714	24,505	261,673	202

a) Core point: if sample x_i contains at least *minPts* samples within radius *r,* then sample point x_i is called the core point.
b) Border Point: if the sample x_i contains fewer than *minPts* samples within the radius *r* but is in the neighbor of other core points, then the sample point x_i is called the boundary point.
c) Noise point: a point that is neither a core point nor a boundary point is generally isolated outside the cluster, which is called an isolated point within this study.

There are some important concepts that need to be explained (Chen et al., 2021):

a) Directly density-reachable: a point *p* is directly density-reachable from a point *q* with respect to {*Eps*, *MinPts*} if $p \in N_{Eps(q)}$ and *q* is a core point.
b) Density-reachable: a point *p* is density-reachable from a point *q* with respect to {*Eps*, *MinPts*} if there is a chain of points p_1, p_2, p_n, with $p_1 = q$ and $p_n = p$ such that p_{i+1} is directly density-reachable from p_i.
c) Density-connected: a point *p* is density-reachable from a point *q* with respect to {*Eps*, *MinPts*} if there is a sample point *o*, and the density of both *p* and *q* can be reached from the sample point *o*.

Where *Eps*(*r*) represents the radius, and the operating principle of DNSCAN is to determine all the core points in a given point set according to the set neighborhood parameters *Eps*(*r*) and *minPts*. Then, starting from the core point, find the cluster formed by all samples with the density of the core point. Finally, this step is repeated until all core points are processed. Finally, points that are not included in any cluster are misidentified as RNBs, and these points need to be excluded to obtain higher recognition accuracy. The algorithm principle of DBSCAN is illustrated in Fig. 7.

3.4.2. Continuous processing of RNBs points

To acquire the measurable mileage and position of RNB, this study constructs a series of continuous line segments based on two consecutive RNB points. According to the collection rule of the BSV images, if the distance between two adjacent RNB points is less than or equal to 20 m,
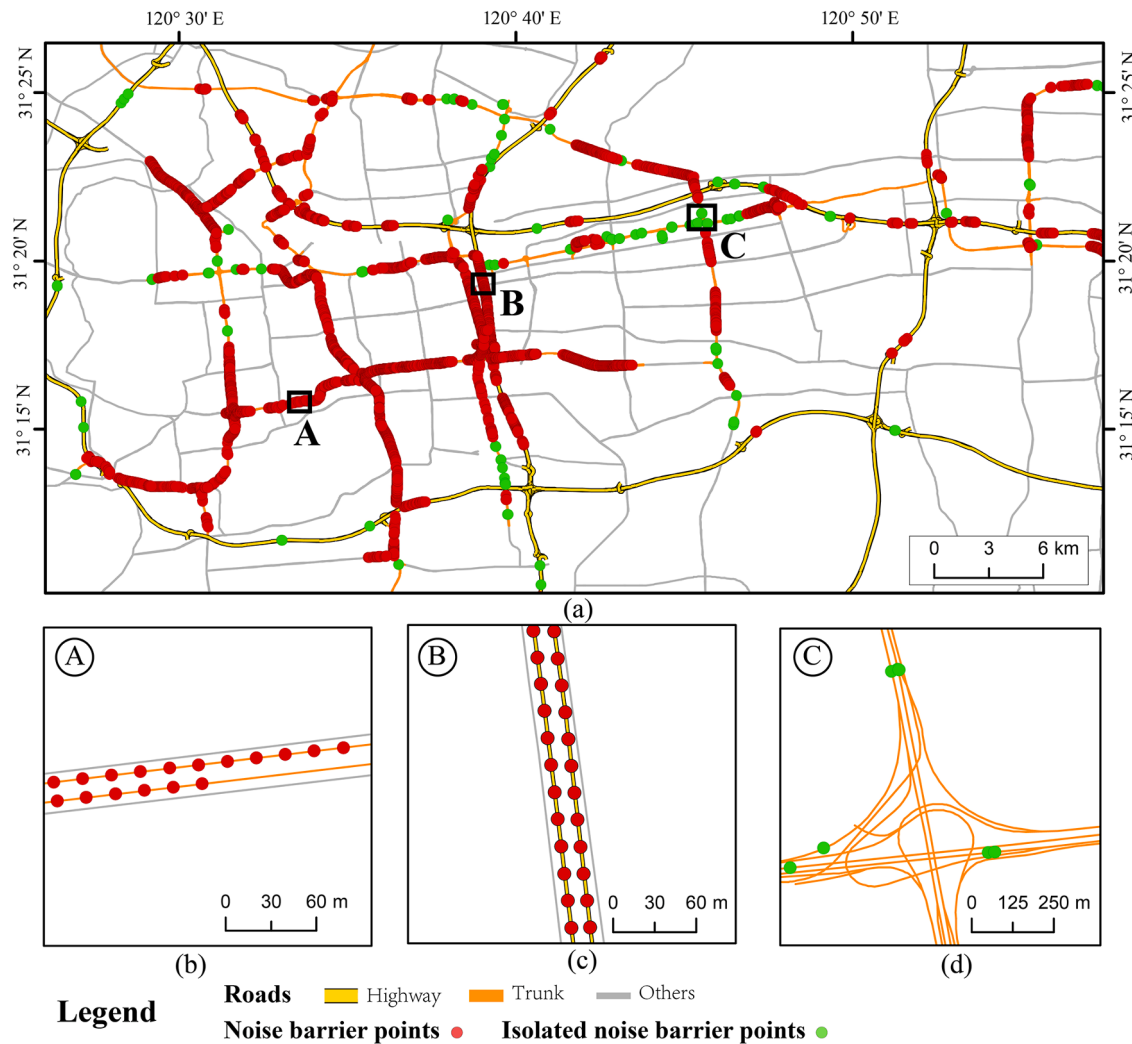
Fig. 8. The RNBs identification results of the ECM of Suzhou. (a) indicates the spatial distribution of the BSV images with RNBs and isolated RNBs points, (b), (c), and (d) are the enlarged areas corresponding to the marked boxes in (a), respectively.

then they will be converted to a continuous line that represents the real distribution of the RNBs. However, when collecting BSV images, the sampling point coordinates need to be converted from World Geodetic System 1984 (WGS 84) to the BD09 coordinate system. The WGS84 is a coordinate system established for the use of the GPS global positioning system. The BD09 is generated by implementing a double encryption algorithm based on the WGS 84 coordinate system. In addition, the distance between these sampling points will slightly deviate due to the transformation of the projection coordinates. Therefore, this study decided that if the distance between two adjacent RNB points is less than or equal to 21 m, they will be connected to a line that represents the real distribution of the RNBs.

4. Experiments results and analysis

4.1. The identification result of RNBs for Suzhou

As a case study in Suzhou, this study demonstrates a method that can accurately identify and match RNBs onto topological road networks for straightforward visualization and is associated with a series of thematic attributes for geospatial analysis. A total of 287,714 BSV images were collected from 2014 to 2020 in Suzhou. The identified results of the RNBs are shown in Table 4 and Fig. 8.

Overall, the constructed ECM identifies 24,505 images with RNBs and 261,673 images without RNBs and misidentifies 202 images. Fig. 8(d)

illustrates the spatial distribution of the misidentified RNB points. We can intuitively observe that these misidentified points are generally scattered along the roads, which does not fit the general distribution situation of the RNBs. According to previous research (Zhang, 2018) , to build RNBs with a length of less than 20 m on a certain road section alone, the costs of construction and maintenance are higher. In fact, most of these isolated points are demonstrated as misclassified RNBs with manual validation. Therefore, according to the method described in Section 3.4, these isolated points were removed. After deleting the isolated points, this study visualizes the remaining BSV images with RNBs onto the map.

As described in Section 3.4, the BSV images with RNBs and points intervals less than or equal to 21 m are connected by a linear distribution of RNBs. The lines represent the real RNB distribution of Suzhou. The results shown in Fig. 9 are the final RNB identification results after completing the ECM experiment and postprocessing based on geospatial analysis.

Fig. 9 shows that the existing RNBs are mainly distributed along the trunk roads in Suzhou. It is reasonable to explain that residential communities, educational facilities, and offices are mostly near the trunk roads of the city for fast and short commuting. This urban-function driven design also has a drawback, i.e., continuous noise made by traffic affects public health in several aspects (Begou, Kassomenos, & Kelessis, 2020). To significantly reduce the noise level, it is imperative to construct RNBs along the trunk road. In comparison, highways are constructed in suburbs far away from the core urban areas with a low-density population, and
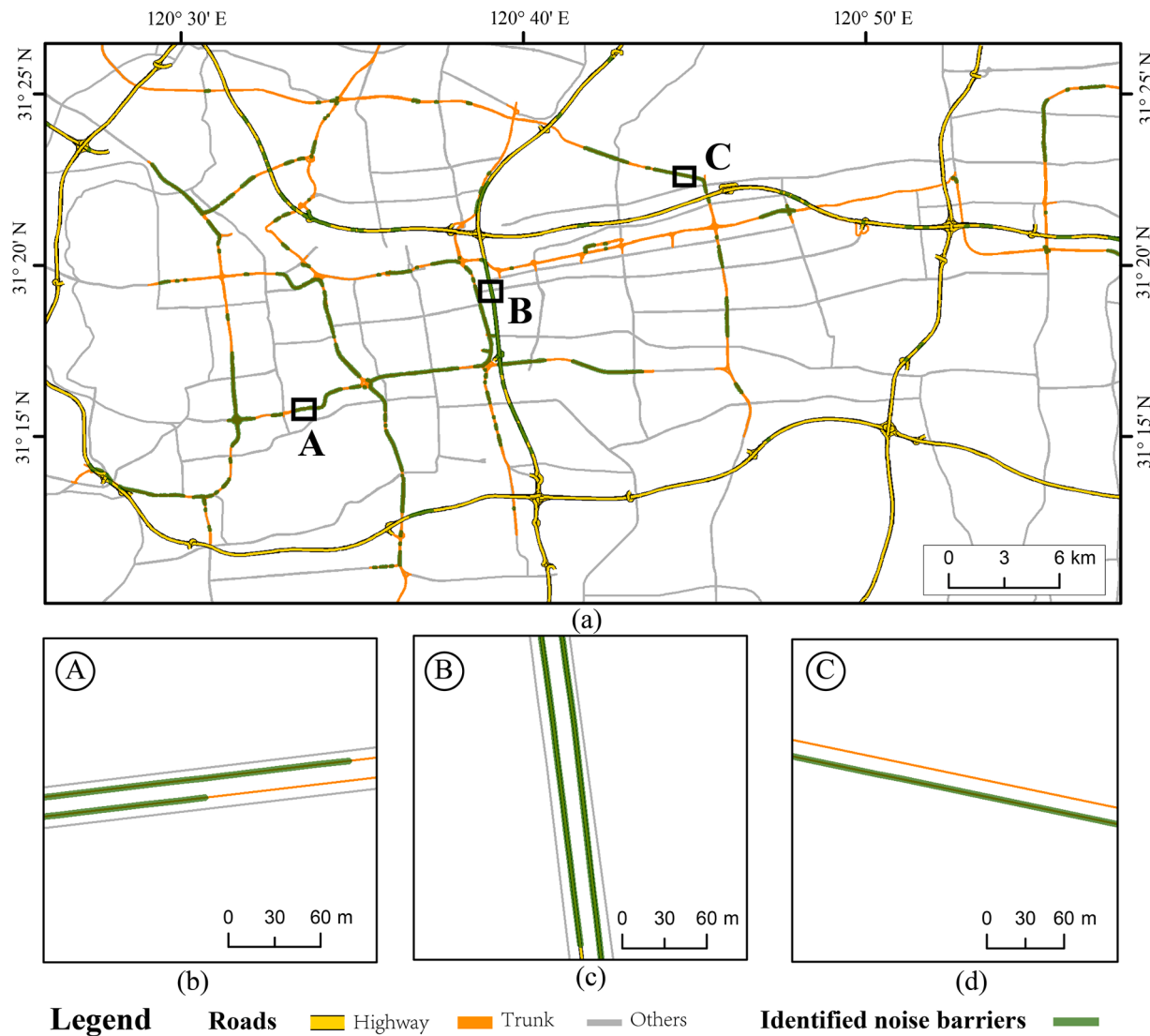
Fig. 9. The spatial distribution of the identified RNBs in Suzhou. (a) indicates the spatial distribution of the RNB, (b), (c), and (d) are the enlarged areas corresponding to the marked boxes in (a), respectively.

Table 5
Conformity between the identification results of Suzhou RNBs and the manually marked results.

Road Name	Start Point	End Point	ECM (m)	Manual (m)	Conformity (%)
Central Circle North Line	Lv Shan Road	Nan Sha Road	805	760	94%
Chang Tai Highway	Xing Hang Road	Suhong West Road	802	802	100%
Nanhuan East Road	South Loop Elevated	Ren Min Road	851	1190	72%

thus, there are fewer areas that need to be deployed with RNBs. The results show that the total mileage of the RNBs in Suzhou is 178,919 m. After a statistical analysis, the RNB mileages distributed along the highway and truck road are 38,863 m and 140,056 m, respectively.

To explore the limitation of the proposed approach of automatically identifying RNBs at city scales, we intend to compare the final identification results of the proposed method with the real distribution of RNBs in Suzhou. First, the total mileage of the RNBs identified by the ECM is statistically analyzed through the OSM ID attributes of the road data and used to make a sequence. Then, the first 3 roads in the sequence are selected to manually measure the positions and mileages of the

existing RNBs with the help of BSV. Because the precise position of each RNB is not easy to identify and relies only on visual judgment, this study selects road intersections as the statistical start and endpoints. Finally, the ECM identification results and BSV measurement results of all road RNBs are separately counted. The selected road information and contrastive results are shown in Table 5.

Table 5 shows that the ECM achieves satisfactory performance regarding the identification of RNBs along the Central North Line and Chang Tai Highway, but on the South Ring East Road, the ECM identification results are still far from the actual distribution of the existing RNBs. After manually locating BSV images belonging to the Nanhuan East Road, the author found that there were many vehicles in the BSV images. It is very likely that the vehicles in the BSV images blocked the RNB, which caused the poor performance of the RNB identification approach proposed in this study for the Nanhuan East Road.

4.2. The limitation of RNBs identification based on SVI and deep learning

The results obtained from this study confirm that ensemble learning and BSV have promising potential to automatically identify RNBs along road networks in a city. The accuracy and F1-score of the ECM RNB identification results were 0.98 ($\pm$ 0.00) and 0.90 ($\pm$ 0.02), respectively. This suggests that RNBs identification results have a high degree of
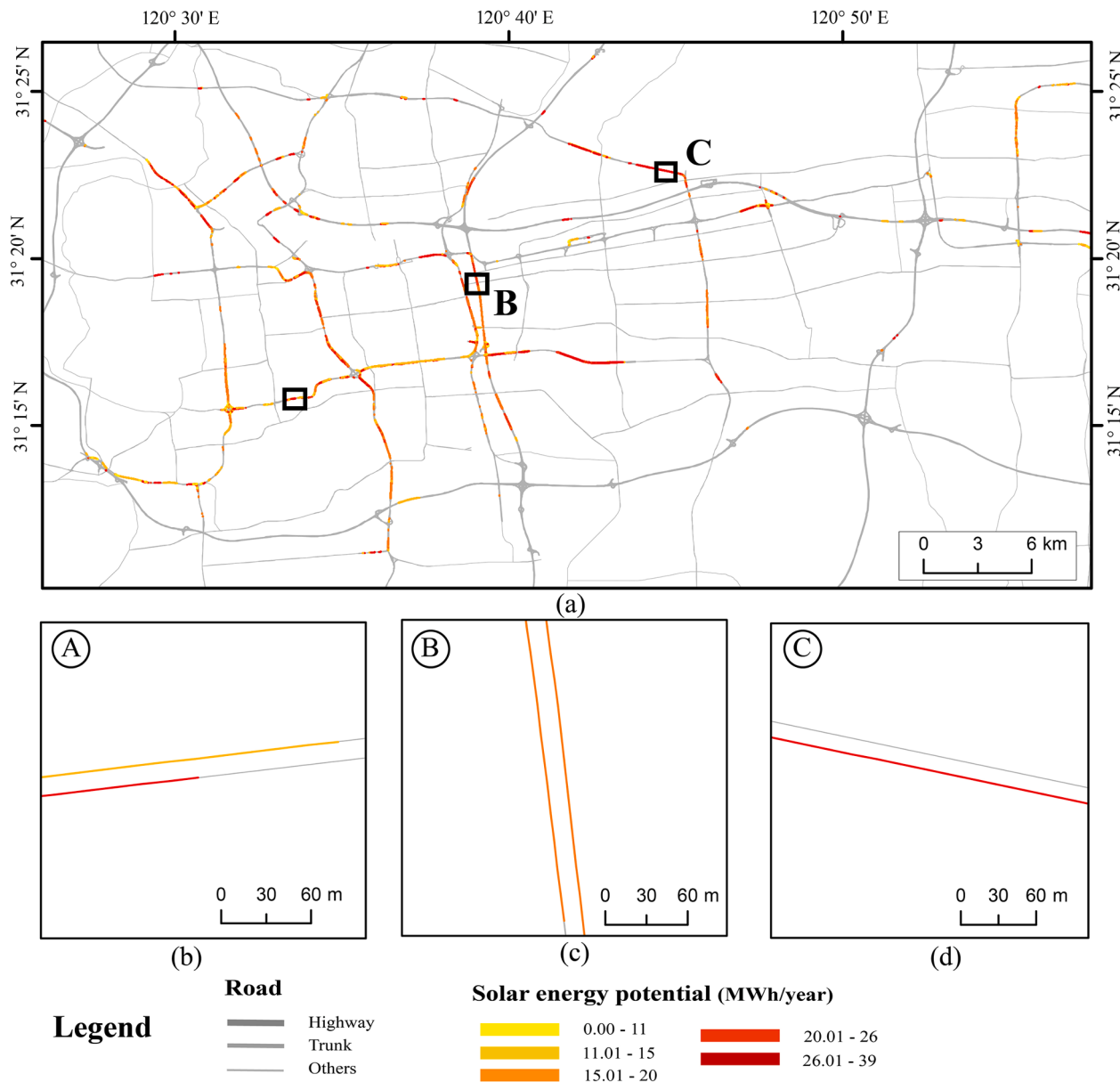
Fig. 10. The spatial distribution of the solar energy potential of RNBs in Suzhou. (a) The solar energy potential of RNBs, (b), (c), and (d) are the enlarged areas corresponding to the marked boxes in (a), respectively.

Table 6
Capacity and electricity power output results of PVNBs in Suzhou.

Road level	Areas of RNBs (m²)	Rated power of PVNBs (W/m²)	Capacity (MW)	Power output (MW h)
Highway	116,589	200	23.3	7022
Truck road	420,358	200	84.1	26,306
Total	536,947	—	107.4	33,328

conformity with the marked RNBs at most road segments. However, the results displayed on the map still exhibit slight deviations from the real distribution of the existing RNB on some road segments. By carefully analyzing all the processes and results, we suggest that some objective factors are regarded as causing unconformity between the identified and marked distributions of RNBs on some roads. The reasons are discussed as follows: 1) Although this study collected all BSV images from 2014 to 2020 in Suzhou, some SVIs were not obtained at some sampling points. This is due to the incompetence of the original SVI data, some of which

were not collected by the operator. 2) Some road segments are fulfilled by different types of vehicles, which blocks the RNBs in the BSV images and then causes difficulty in identifying the RNBs. 3) A few BSV images with RNBs are misclassified by the ECM because they do not contain RNBs. Therefore, these misclassified BSV images will not be displayed on the digital map and will cause the linear distribution of RNBs to be interrupted at these misclassified BSV image points. This shortcoming also suggests that the proposed geospatial analysis method needs to be improved further.

5. RNBs application case

The distribution characteristics of RNBs can be applied in many areas. For example, the number of people who are protected by the RNBs can be statistics based on the impact distance of the traffic noise (Abo-Qudais & Alhiary, 2004). In recent years, RNBs have been regarded as promising locations that can be combined with distributed photovoltaic systems to utilize solar energy. However, there is a challenge in that it is unknown whether the deployment of PVNBs in large

areas can benefit. The solar potential of PVNBs needs to be assessed to acquire the precise position and areas of RNBs (Zhong et al., 2021a). In this study, the precise position and mileage of RNBs have already been collected by ECM and postprocessing based on the geospatial method. According to our former research, the height of the RNBs assumed is 3 m. Then, the area of RNBs can be calculated.

In Suzhou city, the distribution, mileage, and areas of RNBs have already been acquired and deduced. The method of RNBs radiation evaluation can be found in related research (Raptis et al., 2017). Then, a high spatial resolution (10 km) surface solar radiation dataset can be collected from the National Tibetan Plateau Data Center (Feng & Wang, 2021). Since the radiation data are only updated to 2017, in order to be able to characterize the radiation situation in 2020, we have performed a 10-year average of the collected radiation data from 2009 to 2017. Therefore, the 2020 solar energy potential of PVNBs in Suzhou city can be assessed based on the above method and data, and the assessment result is shown in Fig. 10.

The 2020 solar energy potential of RNBs in Suzhou is 208,301MW h based on statistics. The solar energy potentials of highways and trunk roads are 44,062 MW h and 164,239 MW h, respectively. In addition, the capacity and power generated of PVNBs in Suzhou can also be calculated by referring to the parameters of mainstream photovoltaic systems at current markets or related research (Qi, Jiang, Lv, & Yan, 2020). Table 6 illustrates the calculated capacity and power generated for Suzhou's PVNBs.

According to the assessment results of RNBs, combined with the total costs of RNBs and the market price of traditional energy, an economic feasibility assessment of RNBs can be conducted. This will greatly help promote and develop PVNBs. It will accelerate the transformation and upgrading of the urban energy structure, and further promote the sustainable development of urban.

6. Discussion and conclusion

6.1 Discussion

RNBs are important infrastructures in urban areas and are closely related to the planning of urban function districts, assessment of citizen residential environment quality, and exact mapping of urban traffic noise pollution. Additionally, the spatial distribution of RNBs can indirectly reflect some social regulars and patterns of urban areas (e.g., the urban resident's distribution characteristics of rich and poor). Combined with the spatial distribution of RNBs and the footprint of urban buildings, the policy markers and planners can utilize these data to acknowledge which places need to be built RNBs but have not yet been built. The governance of urban road noise is also an important part of the assessment of urban sustainable development. Digitizing the precise position and mileage of existing RNBs and integrating them into the city's digital management platform, it will be profound for smart cities construct. Besides, in the context of the peak carbon and carbon neutral policy in China, PVNBs are a promising approach to help achieve the goal. Therefore, scientific and reasonable planning and improvement of urban road noise barriers will have a positive impact on the improvement of the urban living environment, the well-being of residents' lives, and sustainable urban development.

6.3. Conclusion

This study proposes a method that utilizes SVIs and ensemble learning to obtain the precise positions and mileages of RNBs. The proposed method has been validated by use Suzhou city. The results show that the accuracy of the constructed ECM is 0.98 ($\pm$0.00), and the F1-score is 0.90 ($\pm$0.02), demonstrating that this approach is feasible for conveniently and quickly identifying RNBs at the city scale. This method can effectively compensate for the shortcomings of the precise positions and mileages of RNBs that cannot be easily obtained at the city scale.

Then, this study uses this application case study that assessed the solar energy potential and electricity output of PVNBs to illustrate the importance of RNBs at the urban scale. Since the RNBs and the urban landscape are quite similar in different Chinese cities, the deep learning-based RNBs identification method proposed in this study can be applied in other Chinese cities, indicating a promising opportunity to reveal the spatial distribution patterns of RNBs over a large geographical extent.

Our future study plans to improve the accuracy of RNB identification, make the identification results consistent with the real distribution of urban RNBs and make the RNB measurable so that vital attributes, such as the height and type of RNBs, are based on SVIs. To lay the foundation for a more precise assessment of the solar energy potential of PVNBs and finer mapping of the noise map in the cites.

Declaration of Competing Interest

The authors declare that they have no known competing financial interests or personal relationships that could have appeared to influence the work reported in this paper.

References

Abo-Qudais, S., & Alhiary, A. (2004). Effect of distance from road intersection on developed traffic noise levels. *Canadian Journal of Civil Engineering, 31*(4), 533–538. https://doi.org/10.1139/l04-016

Alam, P., Ahmad, K., Afsar, S., & Akhtar, N. (2020). 3D noise mapping for preselected locations of urban area with and without noise barriers: A case study of Delhi, India. *Noise Mapping, 7*(1), 74–83. https://doi.org/10.1515/noise-2020-0006

Alawi, A., Anaam, E., & Al-sohbani, B. (2021). Performance analysis of deep dense neural networks on traffic signs recognition. *IEEE*, 1–4. https://doi.org/10.1109/ICTSA52017.2021.9406518

Baidu Map Open Platform. (2021). *Web Services API*. https://lbsyun.baidu.com/index.php?title=static. (Accessed 14 December 2021).

Begou, P., Kassomenos, P., & Kelessis, A. (2020). Effects of road traffic noise on the prevalence of cardiovascular diseases: The case of Thessaloniki, Greece. *The Science of the Total Environment, 703*, Article 134477. https://doi.org/10.1016/j.scitotenv.2019.134477

Chang, Y., Abimannan, S., Chiao, H., Lin, C., & Huang, Y. (2020). An ensemble learning based hybrid model and framework for air pollution forecasting. *Environmental Science and Pollution Research International, 27*(30), 38155–38168. https://doi.org/10.1007/s11356-020-09855-1

Chen, Y., Zhou, L., Bouguila, N., Wang, C., Chen, Y., & Du, J. (2021). BLOCK-DBSCAN: Fast clustering for large scale data. *Pattern Recognition, 109*(8), Article 107624. https://doi.org/10.1016/j.patcog.2020.107624

Díez-Pastor, J., Rodríguez, J., García-Osorio, C., & Kuncheva, L. (2015). Random Balance: Ensembles of variable priors classifiers for imbalanced data. *Knowledge-Based Systems, 85*(1), 96–111. https://doi.org/10.1016/j.knosys.2015.04.022

Dong, X., Yu, Z., Cao, W., Shi, Y., & Ma, Q. (2020). A survey on ensemble learning. *Frontiers of Computer Science, 14*(2), 241–258. https://doi.org/10.1007/s11704-019-8208-z

Du, K., Ning, J., & Yan, L. (2020). How long is the sun duration in a street canyon? —— Analysis of the view factors of street canyons. *Building and Environment, 172*(9–10), Article 106680.

Dumbrava, C., & Miah, A. (2016). Assessment and relative sustainability of common types of roadside noise barriers. *Journal of Cleaner Production, 135*, 919–931. https://doi.org/10.1016/j.jclepro.2016.06.107

Feng, F., & Wang, K. (2021). Merging high-resolution satellite surface radiation data with meteorological sunshine duration observations over China from 1983 to 2017. *Remote Sensing, 13*(4), 602. https://doi.org/10.3390/rs13040602

Gebru, T., Krause, J., Wang, Y., Chen, D., Deng, J., Aiden, E., et al. (2017). Using deep learning and Google Street View to estimate the demographic makeup of neighborhoods across the United States. *Proceedings of the National Academy of Sciences of the United States of America, 114*(50), 13108–13113. https://doi.org/10.1073/pnas.1700035114

Zimmerman, R., Panda, A., & Bulović, V. (2020). Techno-economic assessment and deployment strategies for vertically-mounted photovoltaic panels. *Applied Energy, 276*, Article 115149. https://doi.org/10.1016/j.apenergy.2020.115149

He, K., Zhang, X., Ren, S., & Sun, J. (2015,. December 11). *Deep residual learning for image recognition*. Retrieved from http://arxiv.org/pdf/1512.03385v1.

Ghiasi, M., & Zendehboudi, S. (2021). Application of decision tree-based ensemble learning in the classification of breast cancer. *Computers in Biology and Medicine, 128*, Article 104089. https://doi.org/10.1016/j.compbiomed.2020.104089

Government of South Australia Department for Infrastructure and Transport. (2013). *Noise barriers.* https://dpti.sa.gov.au/infrastructure/nsc/south ern_expressway_duplication/project_overview/noise_barriers#locations. (Accessed 14 December 2021).

Hoffmann, E., Wang, Y., Werner, M., Kang, J., & Zhu, X. (2019). Model fusion for building type classification from aerial and street view images. *Remote Sensing, 11* (11), 1259. https://doi.org/10.3390/rs11111259

Huang, G., Li, Y., Pleiss, G., Liu, Z., Hopcroft, J.E., .& Weinberger, K.Q. (2017, April 1). *Snapshot ensembles: Train 1, get M for free.* Retrieved from http://arxiv.org/pdf/170 4.00109v1.

Huang, G., Liu, Z., van der Maaten, L., & Weinberger, K.Q. (2016, August 25). *Densely connected convolutional networks.* Retrieved from http://arxiv.org/pdf/1608.0 6993v5.

Hu, C., Zhang, F., Gong, F., Ratti, C., & Li, X. (2020). Classification and mapping of urban canyon geometry using Google Street View images and deep multitask learning. *Building and Environment, 167*, Article 106424. https://doi.org/10.1016/j.buildenv.2019.106424

Ibrahim, Y., Wang, H., Bai, M., Liu, Z., Wang, J., Yang, Z., et al. (2020). Soft error resilience of deep residual networks for object recognition. *IEEE Access : Practical Innovations, Open Solutions, 8*, 19490–19503. https://doi.org/10.1109/ACCESS.2020.2968129

Kang, Y., Zhang, F., Gao, S., Lin, H., & Liu, Y. (2020). A review of urban physical environment sensing using street view imagery in public health studies. *Annals of GIS, 26*, 261–275. https://doi.org/10.1080/19475683.2020.1791954

Krawczyk, B., Minku, L., Gama, J., Stefanowski, J., & Woźniak, M. (2017). Ensemble learning for data stream analysis: A survey. *Information Fusion, 37*(2), 132–156. https://doi.org/10.1016/j.inffus.2017.02.004

Li, P., Zhang, H., Guo, Z., Lyu, S., Chen, J., Li, W., et al. (2021). Understanding rooftop PV panel semantic segmentation of satellite and aerial images for better using machine learning. *Advances in Applied Energy, 4*(Issue 1), Article 100057. https://doi.org/10.1016/j.adapen.2021.100057

Liu, C., Chen, L., Zhao, W., & Chen, H. (2017). Shape optimization of sound barrier using an isogeometric fast multipole boundary element method in two dimensions. *Engineering Analysis with Boundary Elements, 85*, 142–157. https://doi.org/10.1016/j.enganabound.2017.09.009

Liu, Y., Ma, X., Shu, L., Yang, Q., Zhang, Y., Huo, Z., et al. (2020). Internet of things for noise mapping in smart cities: state of the art and future directions. *IEEE Network, 34* (4), 112–118. https://doi.org/10.1109/MNET.011.1900634

Maimaitijiang, M., Sagan, V., Sidike, P., Hartling, S., Esposito, F., & Fritschi, F. (2020). Soybean yield prediction from UAV using multimodal data fusion and deep learning. *Remote Sensing of Environment, 237*, Article 111599. https://doi.org/10.1016/j.rse.2019.111599

Middel, A., Lukasczyk, J., Zakrzewski, S., Arnold, M., & Maciejewski, R. (2019). Urban form and composition of street canyons: A human-centric big data and deep learning approach. *Landscape and Urban Planning, 183*(3), 122–132. https://doi.org/10.1016/j.landurbplan.2018.12.001

National Bureau of Statistics of China. (2020). *Suzhou statistical yearbook.* Beijing (in Chinese): Beijing Statistical Press.

Pham, K., Kim, D., Park, S., & Choi, H. (2021). Ensemble learning-based classification models for slope stability analysis. *CATENA, 196*, Article 104886. https://doi.org/10.1016/j.catena.2020.104886

Potvin, S., Apparicio, P., & Séguin, A.-. M. (2019). The spatial distribution of noise barriers in Montreal: A barrier to achieve environmental equity. *Transportation Research Part D: Transport and Environment, 72*(1), 83–97. https://doi.org/10.1016/j.trd.2019.04.011

Qi, L., Jiang, M., Lv, Y., & Yan, J. (2020). A celestial motion-based solar photovoltaics installed on a cooling tower. *Energy Conversion and Management, 216*, 112957. https://doi.org/10.1016/j.enconman.2020.112957

Ranasinghe, D., Lee, E., Zhu, Y., Frausto-Vicencio, I., Choi, W., Sun, W., et al. (2019). Effectiveness of vegetation and sound wall-vegetation combination barriers on pollution dispersion from freeways under early morning conditions. *The Science of the Total Environment, 658*, 1549–1558. https://doi.org/10.1016/j.scitotenv.2018.12.159

Raptis, P. I., Kazadzis, S., Psiloglou, B., Kouremeti, N., Kosmopoulos, P., & Kazantzidis, A. (2017). Measurements and model simulations of solar radiation at tilted planes, towards the maximization of energy capture. *Energy, 130*, 570–580. https://doi.org/10.1016/j.energy.2017.04.122

Redondo, J., Peiró-Torres, M., Llinares, C., Bravo, J., Pereira, A., & Amado-Mendes, P. (2021). Correlation between objective and subjective assessment of noise barriers. *Applied Acoustics, 172*(2–3), Article 107640. https://doi.org/10.1016/j.apacoust.2020.107640

Reiter, P., Wehr, R., & Ziegelwanger, H. (2017). Simulation and measurement of noise barrier sound-reflection properties. *Applied Acoustics, 123*(3), 133–142. https://doi.org/10.1016/j.apacoust.2017.03.007

Schepper, E., Van, S., Manca, J., & Thewys, T. (2012). Combining photovoltaics and sound barriers - A feasibility study. *Renewable Energy, 46*, 297–303. https://doi.org/10.1016/j.renene.2012.03.022

Schubert, E., Sander, J., Ester, M., Kriegel, H., & Xu, X. (2017). DBSCAN revisited, revisited: why and how you should (still) use DBSCAN. *ACM Transactions on Database Systems, 42*(3), 1–21. https://doi.org/10.1145/3068335

Song, Y., Thatcher, D., Li, Q., McHugh, T., & Wu, P. (2021). Developing sustainable road infrastructure performance indicators using a model-driven fuzzy spatial multi-criteria decision making method. *Renewable and Sustainable Energy Reviews, 138*(12), Article 110538. https://doi.org/10.1016/j.rser.2020.110538

Silva, R., Ribeiro, M., Moreno, S., Mariani, V., & Coelho, L. (2021). A novel decomposition-ensemble learning framework for multi-step ahead wind energy forecasting. *Energy, 216*, 119174. https://doi.org/10.1016/j.energy.2020.119174

Suthar, K., & He, Q. P. (2021). Multiclass moisture classification in woodchips using IIoT Wi-Fi and machine learning techniques. *Computers & Chemical Engineering, 154*, Article 107445. https://doi.org/10.1016/j.compchemeng.2021.107445

U. S. Department of Transportation Federal Highway Administration. (2019). *Noise Barriers.* https://www.fhwa.dot.gov/environment/noise/noise_barriers/abatement/, 2019. (Accessed 14 December 2021).

Verma, I., Ahuja, R., Meisheri, H., & Dey, L. (2018). *Air pollutant severity prediction using bi-directional lstm network.*

Wadhawan, S., & Pearce, J. (2017). Power and energy potential of mass-scale photovoltaic noise barrier deployment: A case study for the U.S. *Renewable and Sustainable Energy Reviews, 80*, 125–132. https://doi.org/10.1016/j.rser.2017.05.223

Wang, L., Wang, H., Han, X., & Zhou, W. (2021). A novel adaptive density-based spatial clustering of application with noise based on bird swarm optimization algorithm. *Computer Communications, 174*, 205–214. https://doi.org/10.1016/j.comcom.2021.03.021

Wang, S., & Wang, X. (2019). Modeling and analysis of the effects of noise barrier shape and inflow conditions on highway automobiles emission dispersion. *Fluids, 4*(3), 151. https://doi.org/10.3390/fluids4030151

Wang, S., & Wang, X. (2021). Modeling and analysis of highway emission dispersion due to noise barrier and automobile wake effects. *Atmospheric Pollution Research, 12*(1), 67–75. https://doi.org/10.1016/j.apr.2020.08.013

Wang, Z., Wang, Y., & Srinivasan, R. S. (2018). A novel ensemble learning approach to support building energy use prediction. *Energy and Buildings, 159*(1), 109–122. https://doi.org/10.1016/j.enbuild.2017.10.085

Yan, Y., & Ryu, Y. (2021). Exploring Google Street View with deep learning for crop type mapping. *ISPRS Journal of Photogrammetry and Remote Sensing, 171*, 278–296. https://doi.org/10.1016/j.isprsjprs.2020.11.022

Yang, L., Zhang, L., Stettler, M. E. J., Sukitpaneenit, M., Xiao, D., & van Dam, K. H. (2020a). Supporting an integrated transportation infrastructure and public space design: A coupled simulation method for evaluating traffic pollution and microclimate. *Sustainable Cities and Society, 52*(3), Article 101796. https://doi.org/10.1016/j.scs.2019.101796

Yang, W., Yuan, T., & Wang, L. (2020b). Micro-Blog sentiment classification method based on the personality and bagging algorithm. *Future Internet, 12*(4), 75. https://doi.org/10.3390/fi12040075

Ye, C., Zhang, F., Mu, L., Gao, Y., & Liu, Y. (2021). Urban function recognition by integrating social media and street-level imagery. *Environment and Planning B, 48*(6), 1430–1444. https://doi.org/10.1177/2399808320935467

Ye, N., Wang, B., Kita, M., Xie, M., & Cai, W. (2019). Urban commerce distribution analysis based on street view and deep learning. *IEEE access : practical, 7*, 162841–162849. https://doi.org/10.1109/ACCESS.2019.2951294

Yeh, C., Perez, A., Driscoll, A., Azzari, G., Tang, Z., Lobell, D., et al. (2020). Using publicly available satellite imagery and deep learning to understand economic well-being in Africa. *Nature Communications, 11*(1), 2583. https://doi.org/10.1038/s41467-020-16185-w

Yin, X., Liu, Q., Pan, Y., Huang, X., Wu, J., & Wang, X. (2021). Strength of stacking technique of ensemble learning in rockburst prediction with imbalanced data: Comparison of eight single and ensemble models. *Natural Resources Research, 30*(2), 1795–1815. https://doi.org/10.1007/s11053-020-09787-0

Yuan, X., Xie, L., & Abouelenien, M. (2018). A regularized ensemble framework of deep learning for cancer detection from multi-class, imbalanced training data. *Pattern Recognition, 77*(9), 160–172. https://doi.org/10.1016/j.patcog.2017.12.017

Zhang, F., Wu, L., Zhu, Di, & Liu, Y. (2019). Social sensing from street-level imagery: A case study in learning spatio-temporal urban mobility patterns. *ISPRS Journal of Photogrammetry and Remote Sensing, 153*(3), 48–58. https://doi.org/10.1016/j.isprsjprs.2019.04.017

Zhang, L. (2018). The Study on Sound Barrier for Suburban Railway. *China Railway, 8*(6), 107–112.

Zhao, W., Liu, E., Poh, H., Wang, B., Gao, S., Png, C., et al. (2017). 3D traffic noise mapping using unstructured surface mesh representation of buildings and roads. *Applied Acoustics, 127*, 297–304. https://doi.org/10.1016/j.apacoust.2017.06.025

Zhong, T., Zhang, K., Chen, M., Wang, Y., Zhu, R., Zhang, Z., et al. (2021a). Assessment of solar photovoltaic potentials on urban noise barriers using street-view imagery. *Renewable Energy, 168*, 181–194. https://doi.org/10.1016/j.renene.2020.12.044

Zhong, T., Zhang, Z., Chen, M., Zhang, K., Zhou, Z., Zhu, R., et al. (2021b). A city-scale estimation of rooftop solar photovoltaic potential based on deep learning. *Applied Energy, 298*, Article 117132. https://doi.org/10.1016/j.apenergy.2021.117132

Zhou, H., He, S., Cai, Y., Wang, M., & Su, S. (2019). Social inequalities in neighborhood visual walkability: Using street view imagery and deep learning technologies to facilitate healthy city planning. *Sustainable Cities and Society, 50*(s1), Article 101605. https://doi.org/10.1016/j.scs.2019.101605

Zhu, Q., Shang, Q., Hu, H., Yu, H., & Zhong, R. (2021). Structure-aware completion of photogrammetric meshes in urban road environment. *ISPRS Journal of Photogrammetry and Remote Sensing, 175*(3/W4), 56–70. https://doi.org/10.1016/j.isprsjprs.2021.02.010